CWE-8
June 7-11, 2026
London, ON, Canada

Effect of Turbulence Inflow Conditions on Wind Load Prediction for High-Rise Buildings

Hassan Hemida [a], Jose Arbelo Romero [a], Yonggui Li[b]

[a]*Department of Civil Engineering, University of Birmingham, Birmingham, UK, h.hemida@bham.ac.uk, , jma337@student.bham.ac.uk*
[b]*School of Civil Engineering, Hunan University of Science and Technology, Hunan, China, lyg@hnust.edu.cn*

SUMMARY

Accurate prediction of wind loading on high-rise buildings depends strongly on how the atmospheric boundary layer (ABL) is prescribed at the inlet in computational wind engineering simulations. This paper investigates the sensitivity of numerical predictions to inlet boundary condition specification, with particular emphasis on time-dependent turbulence inflow. Wind-tunnel measurements for flow around an isolated high-rise building with an aspect ratio of 1:1:2 are used for validation. A series of simulations based on steady RANS, unsteady RANS, and the scale-adaptive simulation (SAS) framework are performed, with and without synthetic inflow turbulence generated using spectral synthesizer and vortex methods. Results demonstrate that the inclusion of realistic inlet turbulence significantly improves prediction of mean velocity recovery and turbulence kinetic energy in the wake. In particular, SAS combined with synthetic turbulence exhibits behaviour closer to large-eddy simulation, yielding markedly better agreement with experimental data. The study highlights that inlet boundary conditions are a dominant source of uncertainty in CFD-based wind load assessment of high-rise buildings.

Keywords: *Inlet boundary conditions, Wind loading, CFD, LES, High-rise buildings, Wind tunnel experiments.*

1. INTRODUCTION

Wind loading on high-rise buildings is governed by the interaction between the incoming atmospheric boundary layer (ABL) and flow separation around sharp edges and corners, generating shear layers, vortex shedding, and a highly turbulent wake. Peak suctions and cross-wind/torsional responses are particularly sensitive to the unsteady near-field structures that are seeded and modulated by the upstream turbulence field. In Computational Wind Engineering (CWE), how the inflow is specified (mean profile, turbulence intensity and length scales, spectra, spatial coherence, and vertical variation) can therefore propagate directly into predicted surface pressures and integrated loads (base moments, shear forces) and may dominate the error budget if not treated consistently. This has been repeatedly highlighted in the broader evolution of CWE from early RANS studies toward LES-based approaches for wind-load prediction (Tominaga et. al. 2008). The COST 732 Best Practice Guideline for CFD simulation of flows in the urban environment (Franke et. al. 2011) identified the minimum requirements for a successful CFD simulations around buildings. For high-rise building wind loading, the inlet boundary condition is typically intended to represent a target ABL corresponding to a terrain category and meteorological condition (often neutral stratification in engineering practice). It usually comprises mean velocity profile (log-law or power-law), that is often defined by a reference speed at a reference height and a roughness length (or equivalent parameters). Turbulence intensity profile, Reynolds stresses, and integral length scales varying with height are also important parameters. For spectral domain, the energy spectra (e.g., Kaimal-type shapes) and/or temporal correlations, and spatial coherence such as cross-correlation between points (especially important for tall structures and torsion) are needed information. In addition, the inlet ABL must remain horizontally homogeneous in the

computational domain, which requires consistent matching of inlet profile, ground roughness, and wall functions (or resolved near-wall treatment in LES). However, the study did not investigate the relative effect of these parameters on the CFD results. For RANS, the inlet commonly prescribes mean velocity plus turbulence quantities (e.g., k and ε or ω). For LES/WMLES, it additionally requires time-dependent turbulent fluctuations that reproduce targeted statistics and correlations. Lamberti and Gorle (2020) showed that inadequate inflow turbulence can cause long "development lengths," incorrect shear-layer dynamics, and biased pressure fluctuations—precisely the ingredients that govern peak wind loads on tall buildings.

2. NUMERICAL CASE DESCRIPTION

2.1 Experimental description

In order to investigate the effect of the inlet boundary on the wind loading, the data from the wind-tunnel experiment by Ishihara & Hibi (1998) for the flow around a single high-rise building, with a base (b) to width to height (h) ratio of 1:1:2 are used to validate the CFD models. The building was immersed in a simulated atmospheric boundary layer (ABL). The Reynolds number based on the building base and the mean streamwise velocity of the incident flow evaluated at the building height (U_h), where $h = 2$, and $b = 0.16\text{m}$, was 2.4×10^4. The wind velocity was measured using a constant temperature anemometer probe (Dantec 90C10), which measures the three components of the velocity vector. The undisturbed ABL profiles of mean streamwise velocity, standard deviation of velocity in all three directions and shear stress were reported. In terms of the spatial distribution of the flow-field data, a total of 186 measurement locations were recorded. 66 of these points were located in the vertical mid-plane y/b =0 (plane V0), and 60 points were located in each of the horizontal planes z/b =0.125 (plane H1) and z/b =1.25 (plane H10). Where x, y and z are the streamwise, lateral and vertical directions, respectively. For conciseness, only results in the plane V0 and H1 will be presented, yet the data from all measurement locations is used to calculate the evaluation parameters. The relative standard uncertainty in the velocity measurements was not explicitly detailed in the experiment report. However, the anemometer manufacturer guide (Jørgensen, 2001) described the uncertainty of a typical velocity sample including calibration, with 95% confidence assuming a Gaussian error distribution, to be about 3%. This coincides with reports of other experiments performed with the same equipment (Ubertini & Desideri, 2013).

2.2 Computational domain & grid

The computational domain is $24h \times 10h \times 6h$, as illustrated in Figure 1. The blockage ratio is 0.8% and is well below the maximum of 3% recommended by grid design guidelines (Franke & Baklanov, 2007; Tominaga et al., 2008). Though the distance between the windward building facade and the inlet boundary is limited to $3.75h$. This is a mitigation measure to restrict the unintended development of streamwise gradients in the vertical profiles along the empty computational domain upstream the building (Blocken et al., 2007). This mismatch between inlet and incident profiles originates from certain inconsistencies between the selected turbulence model, inlet profiles, wall functions and computational grid (Blocken et al., 2007). A test simulation of an empty computational domain is performed to assess the horizontal homogeneity associated with the boundary layer flow problem and justify the mitigation measure. The grid consists of a structured topology. A blocking strategy was followed to provide a high resolution in the vicinity and wake of the building, as illustrated in Figure 1.c and 1.d. The grid spacing expands away from the building by an expansion ratio of approximately 1.08 to minimise the truncation error in regions of high gradients (Franke & Baklanov, 2007). Table 1 summarises the characteristics of the grids selected. The grid independence analysis is not included herein due to space constraints but was performed following best-practice guidelines for RANS (Menter &

Lechner, 2021) - used in developing Grid1 and Grid2 – and for LES (Menter, 2015), used in Grid 3. The minimum grid size on the building in each grid is denoted by Δ_{min}.

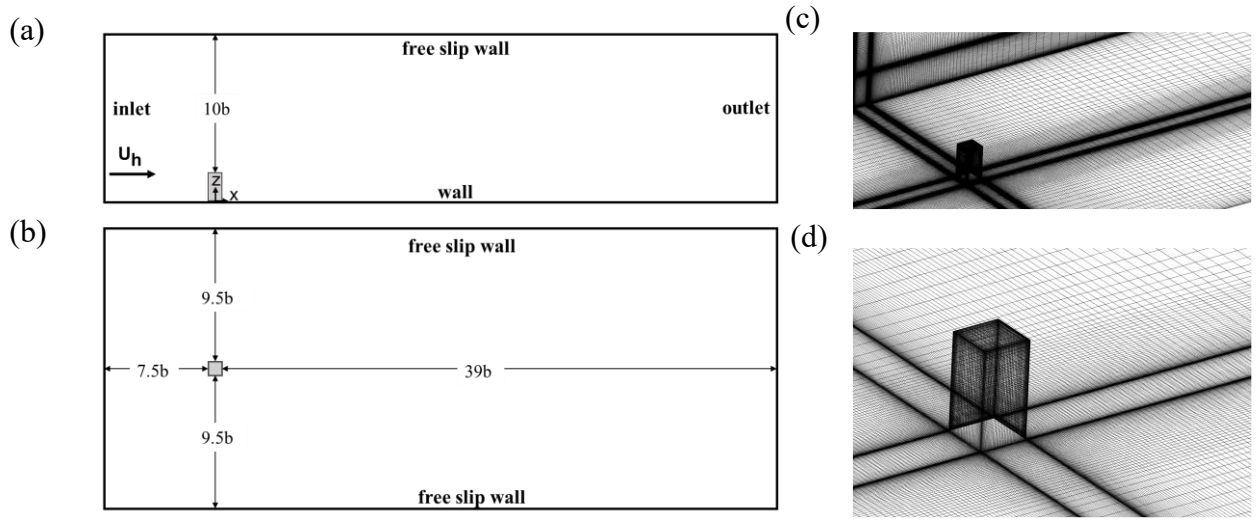

Figure 1. Schematic of computational domain: (a) side view; (b) top-view. (Not to scale). Computational grid discretisation as seen from inlet boundary: (c) zoom out; (d) zoom in.

Table 1 Characteristics of different grids selected

Grid	Cells ($\times 10^6$)	$\Delta_{min}/b(\times 10^{-2})$	$\overline{y^+}$: $building$	$\overline{y^+}$: $floor$
Grid1	2.8	2.5	21.8	27.2
Grid2	7.8	0.625	6.4	7.0
Grid3	7.8	0.625	6.1	6.6

2.3 Boundary conditions & solver settings

The measured incident vertical profiles of streamwise mean velocity (U) and the fluctuating velocity components σ_u, σ_v and σ_w in Ishihara and Hibi (1998) are used to define the inlet boundary condition. The turbulent kinetic energy vertical profile (k) is defined based on the measured standard deviations of the velocity fluctuations, as per $k(z) = 0.5\left({\sigma_u}^2(z) + {\sigma_v}^2(z) + {\sigma_w}^2(z)\right)$. The vertical profile of turbulence dissipation rate (ϵ) is given by $\varepsilon(z) = {u_*}^2 dU/dz$ as derived by Richards & Norris (2011). The friction velocity term is given by $u^* = {C_\mu}^{\frac{1}{4}} {k_p}^{\frac{1}{2}}$, where k_p is the turbulent kinetic energy evaluated at the centre point of wall-adjacent cell (p), and C_μ is an empirical constant with value 0.09 (ANSYS, 2021). The inlet vertical profile of specific dissipation rate $\omega(z)$ is defined from $k(z)$ and $\varepsilon(z)$ through $\omega(z) = \epsilon(z)/C_\mu k(z)$. Free slip boundary conditions are imposed on the side walls and roof. At the outlet, a zero pressure distribution is assumed. Smooth wall functions based on a y^+ insensitive formulation which blends between the analytical expression for ω in the viscous sub-layer and the logarithmic region (ANSYS, 2021) are adopted. A rough no-slip wall was set on the floor using the equivalent sand-grain roughness height (k_s) as defined by (Blocken et al., 2007) for Ansys CFX: $k_s = 29.6 z_0$, where z_0 is the roughness height. For Ansys Fluent: $k_s = 9.793 z_0 / C_r$, where the roughness

constant (C_r) is 0.5. Fitting of the logarithmic law to the inflow ABL velocity profile yields a roughness height of 1.4×10^{-6}m. Several methods exist to generate the background turbulence at the inlet. For the purpose of this study, only the spectral synthesizer (SS) and the vortex method (VM) forcing functions are considered (Fluent, 2023), since they do not require extra simulation time or domain length. The cases studied which included these methods, are performed in ANSYS Fluent 23R1. All other simulations are performed with CFX 21R1.

3 RESULTS

3.1 Model Validation

The cases simulated are listed in Table 2, summarising their main characteristics. SRANS-1, URANS-1 and SAS-1 form part of the turbulence modelling approach sensitivity study. SAS-1, SAS-2 and SAS-3 are compared to assess the sensitivity of the SAS approach to inflow turbulence.

Table 2. Characteristics of the different cases studied

Case	Grid	Turbulence framework	Synthetic turbulence	Δt (s)	CFL mean
SRANS-1	Grid1	SRANS $k-\omega$ SST	-	-	-
URANS-1	Grid2	URANS $k-\omega$ SST	-	2×10^{-4}	0.08
SAS-1	Grid3	SST-SAS	-	2×10^{-4}	0.08
SAS-2	Grid3	SST-SAS	VM	2×10^{-4}	0.08
SAS-3	Grid3	SST-SAS	SS	2×10^{-4}	0.09

The degree of agreement between the numerical results and the experiment are presented by the authors in Romero et.al (2024).

3.2 Turbulence inflow sensitivity

The sensitivity of different time-dependent inlet methods within the SAS framework (SAS-1, SAS-2 and SAS-3) in predicting the flow field around the building is presented in Figure 2. SAS-2 and SAS-3 yield very similar results and therefore only the former is included on the figure for clarity of visualisation purposes. As seen in Figure 2.(a,b), SAS-2 shows very close agreement with experimental measurements for U/U_h. In fact, SAS-2 has the highest validation metric for U (with SAS-3) and for the other two components of velocity. The low velocity regions predicted numerically with SAS-2 agree well with experimental results. However, this is not the case for the SAS-1 model, with large variations evident immediately behind the building. SAS-1 underpredicts the magnitude of U/U_h in the reverse flow region at $x/b = 0.75$ and $x/b = 1.25$, as seen in Figure 2.(a,b). But SAS-1 underpredicts the magnitude of the U/U_h elsewhere in the wake. SAS-1 struggles to accurately capture the shear layer developing at the building height and around the sides, projected towards the wake region ($0.75 \leq x/b \leq 2.0$). SAS-2 also exhibits such limitation, albeit less severely. Because in SAS-2 the behaviour akin to LES predominates (Figure 2), a wider range of turbulence scales are resolved and their effect on the mean flow is better reproduced than by SAS-1. The improvement in prediction capacity of k/U_h^2 of the SAS model by incorporating the VM is clear as seen in Figure 2(c,d), especially since $R^2 = 0.60$ and $R^2 = 0.11$ for SAS-2 and SAS-1 respectively. In SAS-1, the inlet does not generate ambient turbulence and

this seems to cause an underprediction of the wake recovery. The introduction of inflow turbulence, in combination with the high grid and time step resolution, seems to cause the SST-SAS model in SAS-2 to behave more akin to a LES-model judging from the low R_μ in V0 and H1 when compared with those for SAS-1 (see Figure 2). Unlike the SAS-1 model which mostly shows a larger R_μ (i.e., more turbulent fluctuations are modelled rather than resolved) and hence the performance tends more towards URANS model than SAS-2. Thus, ambient turbulence is key to sustaining the LES behaviour, i.e., it cannot be relied solely on the building-induced turbulence and the vortex shedding to generate the appropriate levels of turbulence (as seen in SAS-1). The inclusion of the VM boundary condition especially enhanced the model performance in the far wake.

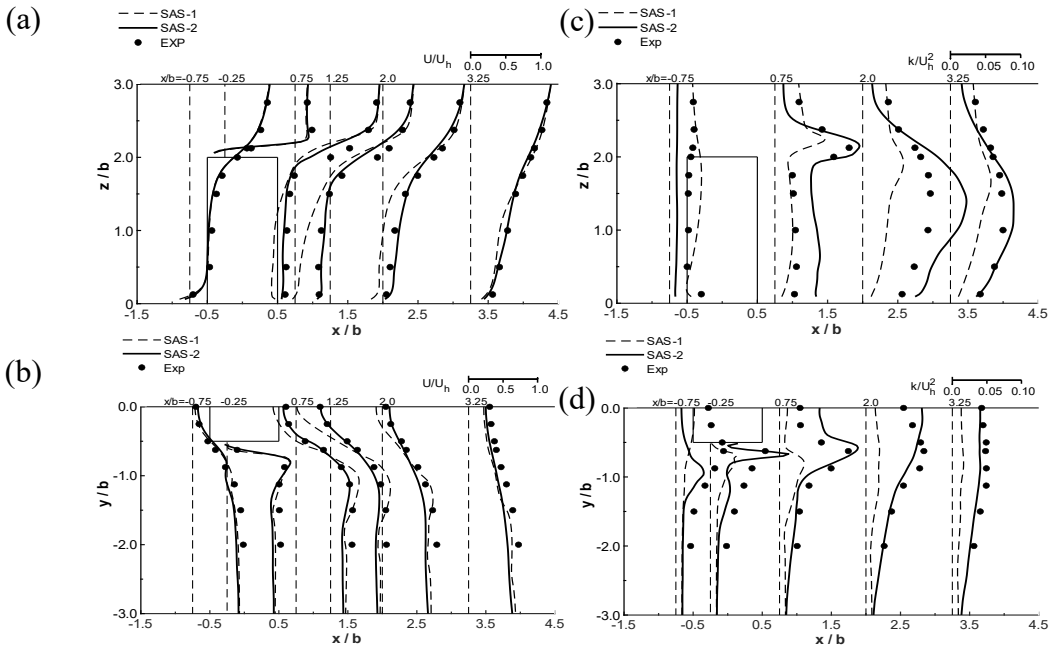

Figure 2 Comparison between the numerical cases SAS-1, SAS-2 and experimental results in terms of: (a) U/U_h in V0; (b) U/U_h in H1; (c) k/U_h^2 in V0; (d) k/U_h^2 in H1

Figure 2.c reveals an observation: the k/U_h^2 profile at $x/b = -0.75$ for SAS-1 exhibits the usual k-profile overprediction due to the stagnation region. But for SAS-2, an almost flat profile with magnitude near 0 is observed, unlike the experimental measurements. Figure 3 shows the k/U_h^2 profile along the intersection line between V0 and H1 planes. The addition of turbulence inflow (blue lines) shifts the peak in k/U_h^2, associated with the horseshoe vortex (forming upstream a building around it's base), further upstream the building. Because of the lack of experimental measurement points in the range $-2.0 \leq x/b \leq -0.5$, the location of the horseshoe vortex cannot be confirmed. However, the k/U_h^2 value at $x/b = -0.75$ obtained numerically with SAS-1, URANS-1 or RANS-1 show closer agreement with measurements than SAS-2 or SAS-3.

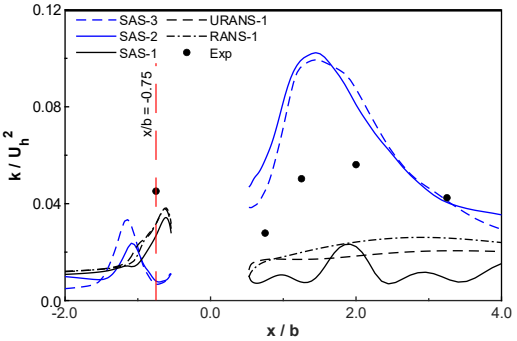

Figure 3 Profile of k/U_h^2 along centreline ($y/b = 0$) on the plane H1. Red line marks location of $x/b = 0.75$.

3.3 Further work

In the full-length paper and conference presentation new surface pressure measurements and numerical simulations using LES for a single and interference buildings with different arrangements will be analysed and presented. In addition, the effect of turbulence length scale at inlet on the building wind loading will be revealed. In addition, various velocity profiles and building orientations will be simulated and analysed.

4. CONCLUSION

The SAS approach with inflow turbulence offers the best agreement with experimental measurements amongst the cases considered herein. But no significant differences in performance were observed between the inflow turbulence techniques considered: spectral synthesizer and vortex method. In the absence of either of these techniques, the URANS backbone predominates in the wake of the building, suggesting building induced unsteadiness is not sufficient to activate the behaviour akin to LES. In terms of statistical convergence, it is shown that local convergence at one or many monitoring points does not guarantee convergence at all locations in flow field.

ACKNOWLEDGEMENTS

All simulations performed on the Birmingham Environment for Academic Research (BEAR) computational facility.

REFERENCES

ANSYS, 2021. Ansys CFX-Solver Theory Guide. Ansys Inc., USA.

Blocken, B., Stathopoulos, T. & Carmeliet, J., 2007. CFD simulation of the atmospheric boundary layer: wall function problems. Atmospheric Environment, January, Volume 41, pp. 238-252.

Fluent, A., 2023. Ansys fluent theory guide. Ansys Inc., USA, Volume 15317.

Franke, J. & Baklanov, A., 2007. Best Practice Guideline for the CFD Simulation of Flows in the Urban Environment: COST Action 732 Quality Assurance and Improvement of Microscale Meteorological Models. s.l.:s.n.

Franke, J., A. Hellsten, K.H. Schlunzen, B. Carissimo 2011. The best practice guideline for CFD simulation of flows in the urban environment: a summary, Int J Environ Pollut, 44, p. 419. 10.1504/IJEP.2011.038443

Ishihara, T. & Hibi, K., 1998. Turbulent measurements of the flow field around a high-rise building. Wind Engineers, JAWE, January, Volume 1998, pp. 55-64.

Jørgensen, F. E., 2001. How to measure turbulence with hot-wire anemometers: a practical guide. s.l.:Dantec.

Jose Romero, Bert Blocken, Hassan Hemida, Mark Sterling, 2024. On the performance of SRANS, URANS and SAS in the prediction of the wind characteristics around a high-rise building, 9th International Colloquium on Bluff Body Aerodynamics and Applications, University of Birmingham, Birmingham, UK.

Lamberti, G. , C. Gorlé, 2020. Inflow sensitivity of LES predictions of wind loads on buildings, J. Wind Eng. Ind. Aerod., 206 (2020), Article 104370

Menter, F. R., 2015. Best practice: scale-resolving simulations in ANSYS CFD. ANSYS Germany .

Menter, F. R. & Lechner, R., 2021. Best practice: RANS Turbulence Modeling in ANSYS CFD. ANSYS Germany .

Richards, P. & Norris, S., 2011. Appropriate boundary conditions for computational wind engineering models revisited. Journal of Wind Engineering and Industrial Aerodynamics , April, Volume 99, pp. 257-266.

Tominaga, Y. et al., 2008. AIJ guidelines for practical applications of CFD to pedestrian wind environment around buildings. Journal of Wind Engineering and Industrial Aerodynamics, October, Volume 96, pp. 1749-1761.

Ubertini, S. & Desideri, U., 2013. Flow development and turbulence length scales within an annular gas turbine exhaust diffuser. Experimental Thermal and Fluid Science, August. pp. 55-70.